Supplementary Information for

Dynamic Visualization of the Phase Transformation Path in $LiFePO_4$ during Delithiation

Liting Yang,[a] Wenbin You,[a] Xuebing Zhao,[a] Huiqiao Guo,[a] Xiao Li,[a] Jie Zhang,[a] Yonggang Wang,*[,b] and Renchao Che*[,a]

[a]Laboratory of Advanced Materials, Department of Materials Science, Fudan University, Shanghai 200438, P. R. China.

[b] Department of Chemistry and Shanghai Key Laboratory of Molecular Catalysis and Innovative Materials, Institute of New Energy, iChEM (Collaborative Innovation Center of Chemistry for Energy Materials), Fudan University, Shanghai 200438, P. R. China.

1. Materials characterization

The morphologies of LFP was characterized using a field-emission scanning electron microscope (FESEM, Hitachi S-4800, Japan). The micro-size solid-state battery was fabricated on the focus ion beam microscope (FIB, ThermoFisher Helios G4 CX, United States). In situ microstructure evolution of LFP particle was recorded on a field-emission transmission electron microscope (FETEM, JEOL JEM–2100F, Japan) equipped with a postcolumn Gatan imaging filter (GIF, Tridium 863, United States) system working at 200 kV. In situ EELS were conducted in the JEM-2100F TEM. The XRD patterns were obtained by a diffractometer (Bruker D8 Advance, Germany). At last, the linear sweep voltammetry of the micro-sized solid-state battery was examined with electrochemical workstations (Gamry, Reference 600+, United States).

2. Discussion about x-ray diffraction (XRD) of pristine $LiFePO_4$ (LFP)

The sharp diffraction peaks at 17.1°, 20.8°, 25.6°, 29.7°, and 35.6° can be indexed to (200), (101), (111), (020) and (311) respectively, which are assigned to the pure phase of LFP (PDF #83-2092), indicating that the LFP have high-quality crystalline.

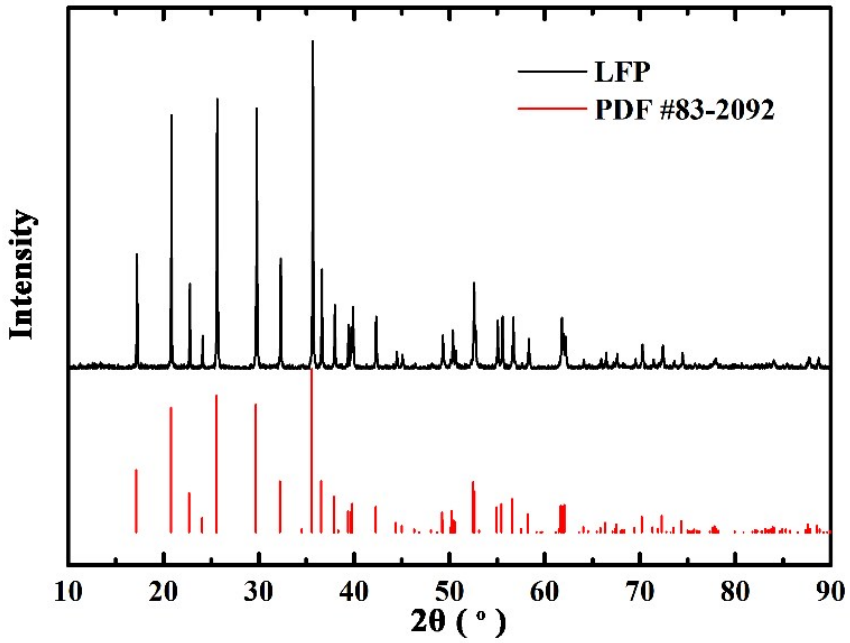

Figure. S1. XRD pattern of LFP.

3. Discussion about scanning electron microscopy (SEM) and transmission electron microscopy (TEM) images of LFP cathode

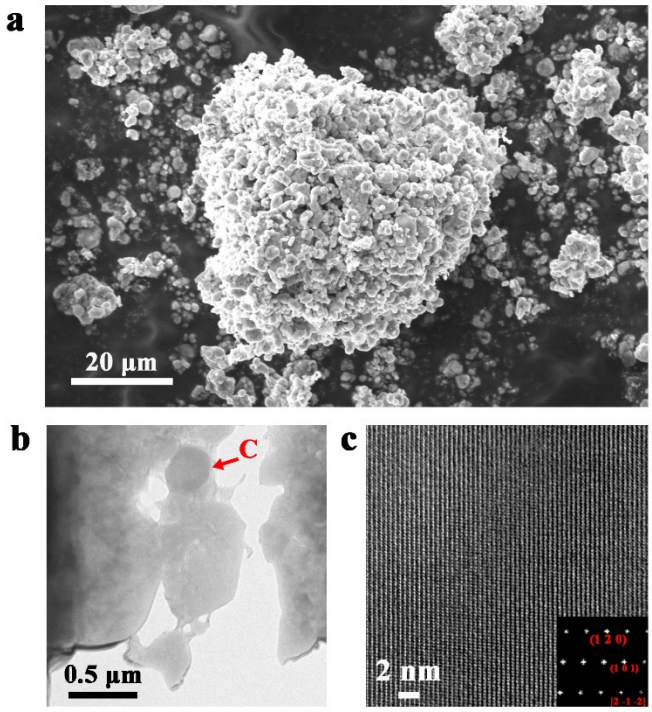

Figure. S2. Representative SEM image and TEM images of LFP cathode. (a) The SEM image of LFP cathode, demonstrating that the LFP cathode is composed of many LFP particle with a broad distribution of particle size. Scale bar, 20 μm. (b) The TEM image of LFP particles. The red arrow indicates the carbon, which coats on the LFP nanoparticles. (c) The high-resolution TEM image of LFP. The inset is the two-dimensional fast Fourier transform derived from the high-resolution TEM image, which can be indexed at the [2 $\bar{1}$ $\bar{2}$] zone axis. Scale bar, 2 nm.

4. The detailed fabrication process of micro-size solid-state battery

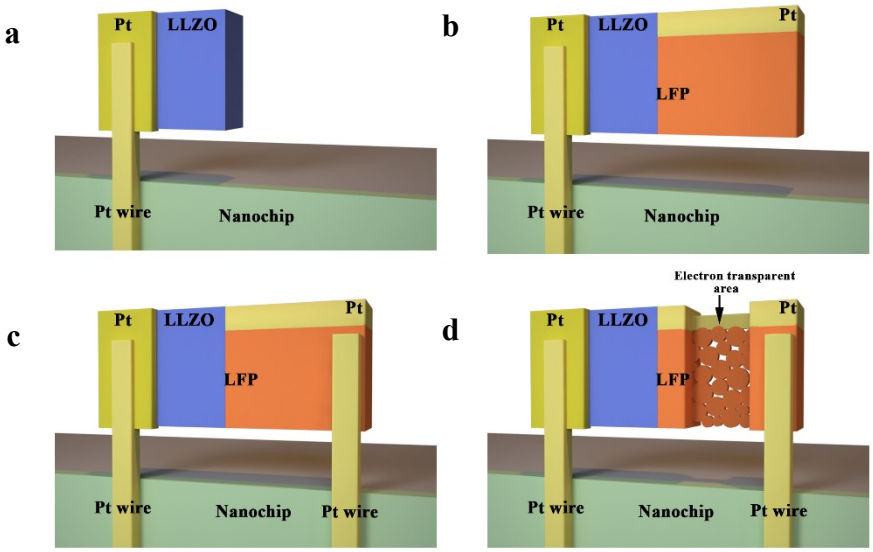

Figure. S3. Schematic process for fabricating solid-state battery by focused ion beam (FIB). (a) A lamellae of $Li_{6.4}La_3Zr_{1.4}Ta_6O_{12}$ (LLZTO) was obtained using the standard TEM specimen preparation technique by FIB[1] and fixed to the nanochip by Pt using ion beam induced deposition. (b) A nanomanipulator was employed to transfer LFP lamellae to LLZTO lamellae (30 kV, 24 pA). Electron beam deposited Pt with poor resistivity comparing to ion beam deposited Pt[2] was used to connect LLZTO with LFP (5 kV, 3.2 nA). (c) Further deposition of ion beam deposited Pt was employed to fasten the solid-state battery to the nanochip (30 kV, 80 pA). (d) LFP cathode was thinned to the thickness of ~100 nm for electron transparency by FIB milling (5 kV, 40 pA and then 2 kV, 15 pA). Both Pt wires on the right side and on the left side act as conductor and fixing the battery to the nanochip. To prevent short circuit caused by Pt deposition contamination, a FIB milling cleaning was carried out on the LLZTO surface after Pt deposition (5 kV, 40 pA).

5. SEM images of a nanochip

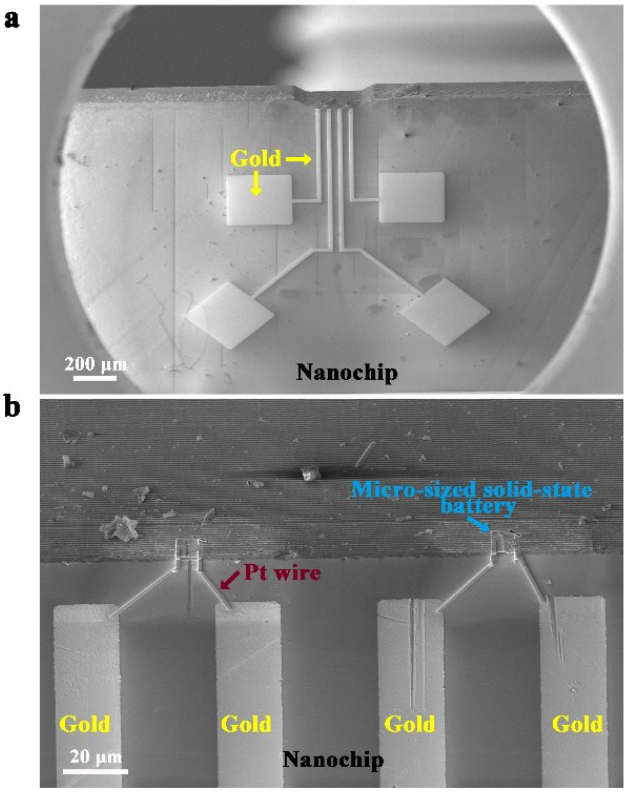

Figure. S4. SEM images of a nanochip. (a) SEM image of a nanochip. These electric circuits on the nanochip are gold fires, which connect to an electrochemical workstation outside TEM column. Scale bar, 200 μm. (b) Magnified SEM image of a nanochip with two micro-sized solid-state batteries. Pt wires using ion beam induced deposition are employed to fix solid-state batteries to the nanochip and also act as conducting wires connecting the micro-sized solid-state battery to the electric circuits on the nanochip. Scale bar, 20 μm.

6. Discussion about in situ selected area electron diffraction (SAED) patterns of the LFP particle

During delithiation, the phase structure of LFP cathode was investigated using in situ SAED. The SAED pattern (Figure. S5b) obtained from the red circle in the TEM image of LFP (Figure. S5a), with one set of 4-fold symmetry diffraction spots, is indexed as [001] zone axis. This result demonstrates these pristine LFP are monocrystalline, in line with XRD and HRTEM characterizations. The lattice spacing of the (300) plane for LFP is 3.40 Å. In addition, diffraction spots (Figure. S5d) of completed-delithiation LFP (Figure. S5c) is indexed as FP, which indicates the existence of phase transformation from LFP to FP during delithiation. The lattice spacing of the (300) plane of FP is 3.22 Å, showing that the lattice spacing of (100) plane decreased about 5.29% after Li extracted from LFP. The same phase structure transformation was obtained in the in situ SAED patterns of other LFP particle during delithiation, as shown in Figure. S6.

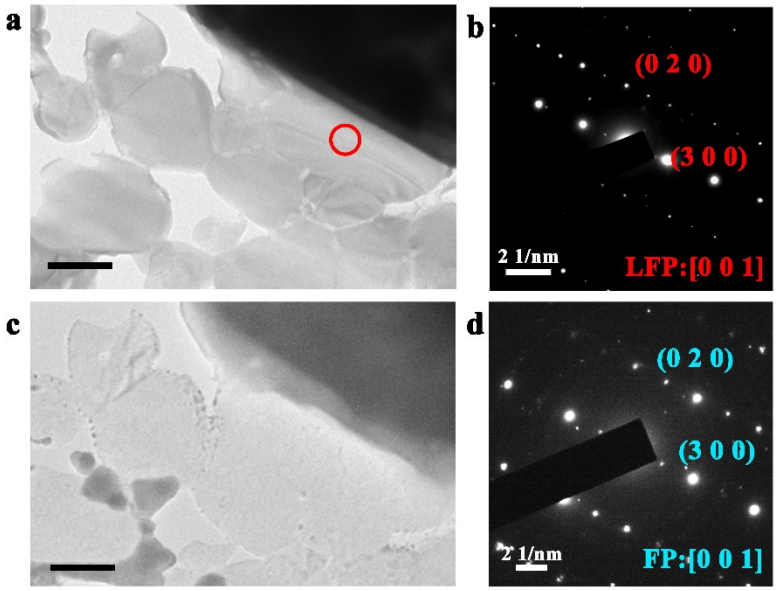

Figure. S5. In situ SAED patterns of the LFP particle during delithiation. TEM images of pristine LFP particles (a), delithiated LFP particles (c). Scale bar, 100 nm. (b,d) Corresponding in situ SAED patterns from the same area marked by red circle in a. Pristine LFP SAED is shown in b. Diffraction spots indexed by the red and blue colors belong to LFP and delithiated LFP, respectively. Scale bar, 2 1/nm.

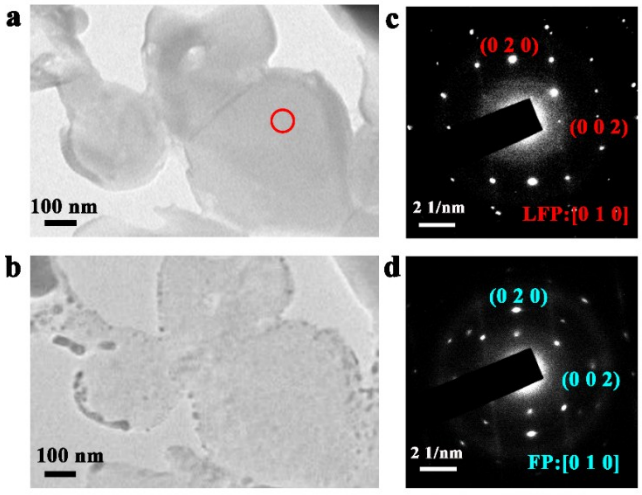

Figure. S6. In situ SAED patterns of the LFP particle during delithiation progress. TEM images of pristine LFP particles (a), delithiated LFP particles (b). Scale bar, 100 nm. (c,d) Corresponding in situ SAED patterns from the same area marked by the

red circle in a. Scale bar, 2 1/nm. Pristine LFP SAED along the [001] zone axis is shown in c; diffraction spots of delithiated LFP in d is indexed as FP, demonstrating the phase transformation from LFP to FP with the Li extraction. The lattice spacing of (020) plane of LFP and FP are 2.89 Å and 2.99 Å, respectively. This result shows the interplanar spacing of (020) decreased about 3.34%. Diffraction spots indexed by red and blue colours belong to LFP and delithiated LFP, respectively.

7. Characterization of delithiated LFP particles relaxed for 24 hour

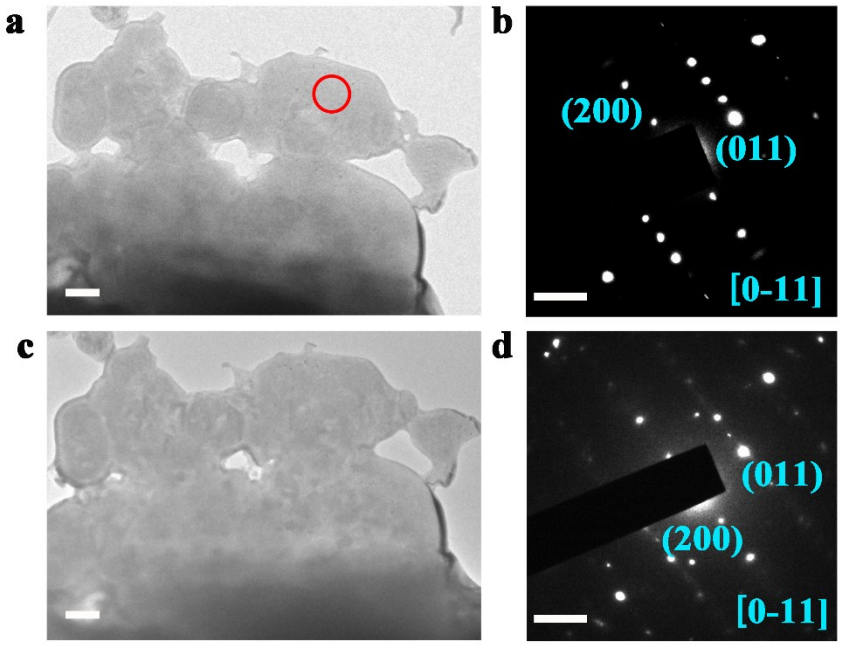

Figure. S7. Microstructure and phase structure evolution of delithiated LFP particles relaxed for 24 hours. TEM images of delithiated LFP particles (a), relaxed delithiated LFP particles (c). Scale bar, 200 nm. (b,d) Corresponding SAED patterns from the same area marked by the red circle in a. Scale bar, 2 1/nm. The delithiated LFP particles are verified to be FP through corresponding SAED pattern, which can be indexed at the [0 -1 1] zone axis. After relaxed for 24 h, the SAED pattern of the particle can be indexed as FP without the presence of sharp phase boundaries, indicating that LFP phase transformed into FP phase completely during delithiation.

8. Discussion about electron energy loss spectroscopy (EELS) of pristine LFP and complete-delithiated LFP (i.e. $FePO_4$, FP)

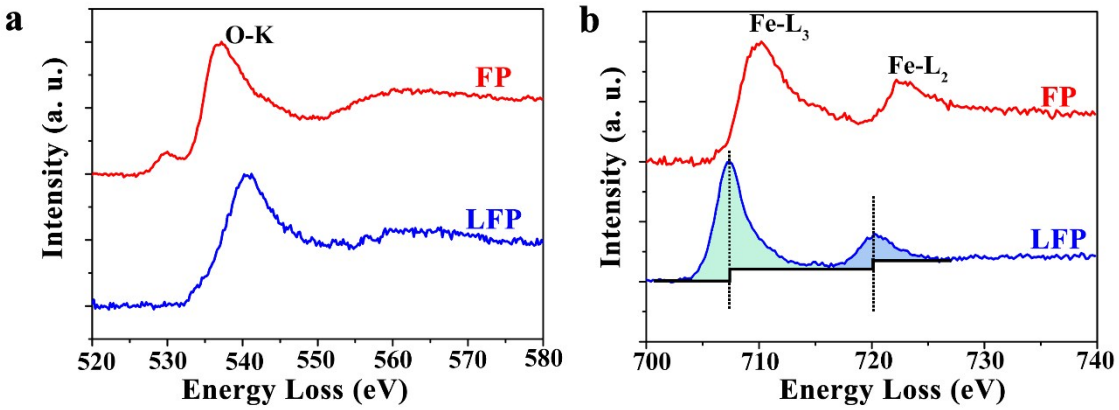

Figure. S8. O-K and Fe-$L_{2,3}$ EELS spectra for FP and LFP. (a) O-K EELS spectra for FP and LFP. The pre-peak of O-K edge is a characteristic feature for Fe^{3+}.[3] The appearance of the pre-peak in O-K spectra indicates the formation of Fe^{3+}-containing phase. (b) Fe-$L_{2,3}$ EELS spectra for FP and LFP. Generally, the integral Fe-$L_{2,3}$ edges white-line intensity ratio $I(L_3)/I(L_2)$ increases with the iron valence state.[4] Therefore, Fe-$L_{2,3}$ EEL spectra can be used to analyze the evolution of the Fe valence state, quantitatively. Fe L_3/L_2-edge ratios for LFP and FP were calculated to be 4.35 and 5.95 based on the Pearson method,[5] which is shown in b.

9. GPA method

The GPA method is a powerful technique to measure and map displacement fields and strain fields basing on HRTEM images of materials. The method uses the spatial frequency components to reveal the local variations in HRTEM images. Firstly, the Fourier transform is performed to the HRTEM image to obtain strong Bragg-reflections, which are related to the crystalline structure. Secondly, a small aperture is applied to a strong Bragg-reflection and an inverse Fourier transform is performed to form a 2D lattice image, which can provide the information of local distortion. Finally, when the method is applied to two non-collinear Fourier components, the displacement field can be derived and the strain components can be derived from the displacement field. In the image of the displacement field, two discontinuities of 2π represent the existence of the dislocations.

References

1 J. Mayer, L. A. Giannuzzi, T. Kamino, J. Michael, *MRS Bull.,* 2011, **32**, 400.
2 D. Brunel, D. Troadec, D. Hourlier, D. Deresmes, M. Zdrojek, T. Mélin, *Microelectron. Eng.,* 2011, **88**, 1569.
3 L. Laffont, C. Delacourt, P. Gibot, M. Y. Wu, P. Kooyman, C. Masquelier, J. M. Tarascon, *Chem. Mater.,* 2006, **18**, 5520.
4 R. D. Leapman, L. A. Grunes, P. L. Fejes, *Phys. Rev. B,* 1982, **26**, 614.
5 D. Pearson, C. Ahn, B. Fultz, *Phys. Rev. B,* 1993, **47**, 8471